Representative and Statistical Volume Elements for Grain Boundary Networks: A Stereological Approach

Tyler R. Critchfield[a], Oliver K. Johnson[a,*]

[a] *Department of Mechanical Engineering*
Brigham Young University, Provo, UT 84602, USA

Abstract

Experimental and computational studies have demonstrated that the structure of grain boundary networks (GBNs), e.g. the connectivity of certain types of grain boundaries (GBs), has a significant impact on macroscopic material properties. Because minor changes in GBN structure can cause large changes in effective properties, it is common to use large microstructures or report averages over many microstructural instantiations with the assumption that results become more representative as the size or number of samples increases. For crystallographic texture, and composite materials, such ideas have been made rigorous through the definition of representative volume elements (RVEs) and statistical volume elements (SVEs). However, for GBNs, the size of an RVE and the cardinality of a set of SVEs have not yet been determined. In this study, we employ stereological methods to evaluate the convergence of triple junction fractions in both idealized and realistic 2D GBNs to quantitatively define RVEs and SVE sets for GBNs. We compare these results to those for crystallographic texture in the same polycrystals and find that the trends for GBNs and texture are remarkably different. Because the vast majority of experimental work currently relies on 2D microstructure characterization, the results obtained for 2D systems have great practical value in and of themselves. However, the stereological approach employed also allows us to make quantitative predictions of RVEs and SVEs for fully 3D microstructures. These results are expected to aid future experimental and computational work in selecting appropriately sized material volumes to achieve robust quantitative results.

Keywords: Grain Boundary, Grain Boundary Network, Representative Volume Element, Statistical Volume Element, Crystallographic Texture

1. Introduction

A representative volume element (RVE) is a volume of material whose properties match—or are representative of—the macroscopic properties of the larger material from which it was taken. While the definition of an RVE still varies within the scientific community, it is generally concluded to be the smallest volume for which this correspondence occurs [1–15], thus, any sample whose size is greater than the RVE must also represent the macroscopic material. The use of an RVE facilitates accurate simulations and experiments while minimizing computational cost and experimental effort. It is also important to note that RVE size depends on the physical property or microstructural attribute being observed [2–4, 13–15].

*Corresponding author.
Email address: ojohnson@byu.edu (Oliver K. Johnson)

While an RVE is smaller and more efficient to use than the complete microstructure, in many cases it may still be too large for practical use. The RVE must capture all important microstructural characteristics of the material at any random location in the structure and must be large enough to prevent rare heterogeneities from being over- or under-represented. Statistical volume elements (SVEs) present an alternative solution to this problem. An SVE is a smaller sample than an RVE and thus does not represent the macroscopic material on its own. However, the aggregate properties of a set of SVEs are representative of the material [1, 10, 14, 16, 17]. With this definition, any sample size can be considered an SVE if the set is comprised of enough samples to ensure that their average accurately represents the macroscopic properties. Smaller sample sizes exhibit more variation in their properties and thus a greater number are required to constitute an SVE set [1, 3, 14, 16, 18, 19]. We refer to the number of samples in an SVE set as the SVE set *cardinality*.

The grain boundary network (GBN) is an important structural characteristic of materials that significantly influences many material properties [20–23]. Modification of the types and arrangement of grain boundaries can result in large changes to the effective properties of a material [24, 25]. Extensive work has been done to investigate GBN structure-property relationships, but quantitative models are limited in number. To draw accurate conclusions regarding GBN structure-property relationships, computational and experimental work should employ an RVE or a set of SVEs. Although the size of RVEs for many material properties have been determined [3, 4, 8, 9, 11, 26, 27], the size of RVEs and the cardinality of SVE sets for GBNs, and properties that are sensitive to them, have not yet been determined. Understanding the nature of RVEs and SVEs for GBNs will enable researchers to generate and quantitatively analyze microstructural data. For instance, the availability of 3D microstructural data sets has recently increased [28] and this trend is expected to continue. While the value of such data sets cannot be overstated, current experimental constraints lead to size limitations that require serious consideration during the experimental design phase and the subsequent data analysis. The same is often true in computational microstructure studies (e.g. atomistic polycrystals). GBN RVE findings will aid in this process and facilitate quantitative conclusions for physical phenomena involving GBNs. In this study, we employ stereological methods to investigate the size of RVEs and the cardinality of SVE sets for 2D GBNs in polycrystalline materials. We also compare these results to the size of RVEs and the cardinality of SVE sets for crystallographic texture in the same microstructures. Leveraging the stereological foundation of our approach, we also make quantitative predictions of RVEs and SVEs for fully 3D microstructures, under a wide range of conditions.

2. Method

2.1. Preliminaries

Idealized 2D honeycomb microstructures (Fig. 1(a)) containing 99,068 grains (roughly 10^5) were generated, similar to those employed in [20, 29–34]. Grains possessed cubic crystal symmetry and all orientations shared a $\langle 001 \rangle$ rotation axis. Additionally, a front-tracking grain growth code, written by Jeremy Mason and based on the algorithm of [35], was used to generate microstructures that resembled more realistic polycrystals (Fig. 1(b)) each having between 99,997–10,000 grains (again roughly 10^5). These two types of microstructures will be referred to as honeycomb and grain growth microstructures, respectively. For both types of microstructures, grain orientations were assigned—using a procedure that will be described below—and GB disorientations were computed. GBs were subsequently classified as special or general based on the Brandon criterion (i.e. low-angle boundaries whose disorientations were less than 15 degrees were considered special) [36, 37].

It has been observed that increasing the population of these special grain boundaries in a material enhances its properties (e.g., resistance to intergranular cracking and hydrogen embrittlement) [21, 22,

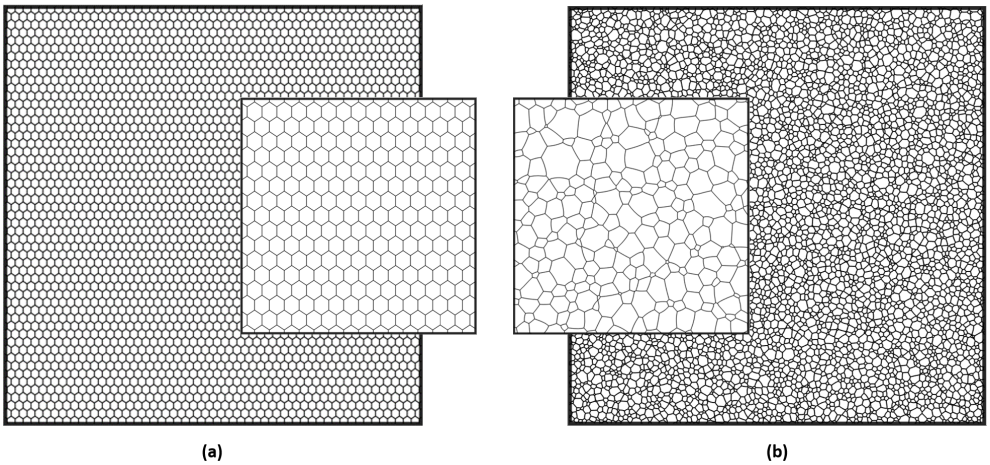

Figure 1: (a) An idealized 2D honeycomb microstructure (at 6× and 20× magnification) and (b) a more realistic 2D microstructure created from a grain growth algorithm (at 4× and 20× magnification).

32]. However, an increase in the percentage of special boundaries is not necessarily sufficient to improve material properties [29, 31, 38]. The fraction of special boundaries does not account for naturally occurring correlations in the GBN. For example, cracks that propagate along general boundaries need only a single connected path to transit the entire microstructure, resulting in fracture. The fraction of special or general boundaries does not encode their spatial arrangement, which can result in widely varying properties even for GBNs with identical special fractions. To account for connectedness between GB types, we use triple junction (TJ) types, and their respective populations, to characterize the connectivity of the GBN [29–31, 38]. TJ fractions of type $\{J_i|\ i\ \epsilon\ \{0,1,2,3\}\}$ denote the proportion of TJs in a microstructure coordinated by i special boundaries. For example, in a microstructure with $J_1 = 50\%$, half of its TJs would contain one special GB (and two general GBs). Microstructures characterized by high J_2 and J_3 concentrations break up the connectivity of general GBs, and thus inhibit processes such as electromigration and crack propagation [25].

These TJ fractions can be represented in a tetrahedral configuration space similar to a quaternary phase-diagram (we will refer to this as the J-space), where each vertex represents a microstructure composed of 100% of the corresponding TJ type [30]. To investigate the influence of TJ fraction on RVE size and SVE set cardinality, and to consider a diverse set of microstructures, we generated microstructures spanning the J-space. Figure 2 shows representative GBNs at several points throughout this space. The J-space was binned, and a Simulated Annealing program was used to obtain microstructures with TJ fractions in each bin [39]. This program takes a microstructure with an initial random assignment of grain orientations and, at each Monte Carlo step, accepts or rejects random changes to grain orientations until the desired TJ fractions of the microstructure are obtained, while preserving crystallographic constraints. A total of 1388 and 1394 bins, spanning roughly 78% of the J-space, were successfully reached for the honeycomb and grain growth templates, respectively. We repeated this process 19 times for both the honeycomb and grain growth templates, so that we obtained 19 different microstructures of each type of template in each bin, for a total of 26,372 and 26,486 microstructures for each type of template. The bins that were not reached are situated near the J_0/J_3 edge, which cannot be be reached using finite microstructures, and near the J_2 corner, which can technically be constructed using finite microstructures, but which are apparently difficult to generate by random grain reorientations.

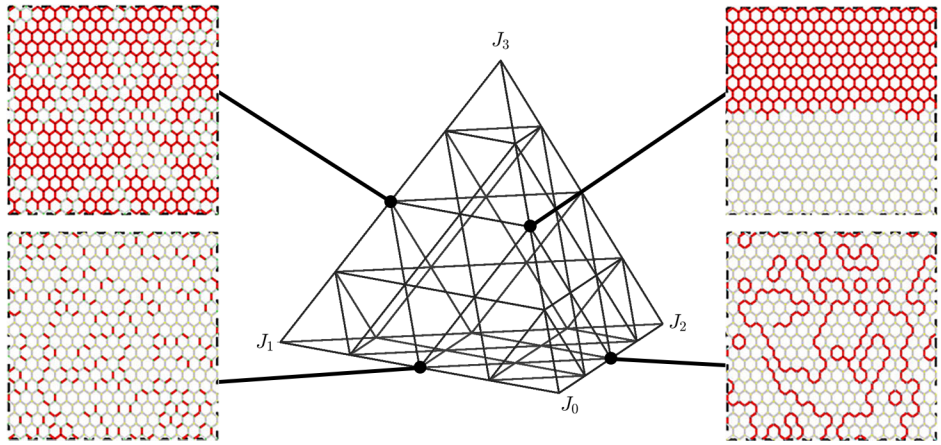

Figure 2: The J-space encompasses every possible triple junction fraction. Each vertex represents microstructures with all triple junctions of that respective type. Sample honeycomb microstructures are shown, with grain boundaries colored as special (red) and general (gray). There are many configurations of special and general boundaries for each triple junction fraction, of which these are examples.

2.2. RVE Characterization

Methods to determine RVE size include numerical and statistical approaches, as well as experimental testing [3, 8, 40, 13, 26, 27]. Our strategy for determining the GBN RVE is based on stereological methods and is depicted graphically in Fig. 3. For each microstructure, samples of increasing size were taken at random locations (represented by the square regions with dashed boundaries in Fig. 3). The TJ fractions were computed as the number of TJs of each type observed within the sample area divided by the total number of TJs observed within the sample area. In stereological notation,

$$J_i = P_{P,i} \tag{1}$$

where $P_{P,i}$ denotes the point fraction (points/points) of TJs of the i-th type. The RVE size was defined as the sample size—expressed in units of number of grains—for which *all* four TJ fractions of the sample converged to the true value of the larger original microstructure. The criterion used for convergence was the size at which the difference between the sample TJ fractions and those of the entire microstructure was within a selected margin of error (1%, 2%, 5% and 10% were used), and where the TJ fractions of every larger sample size were also within the margin of error.

Because TJ fractions can be, and frequently are, equal to zero, the typical definition of relative error is undefined. However, since TJ fractions are by definition in the range $[0, 1]$ the absolute error, which is defined even when $J_i^{\text{true}} = 0$, is also in $[0, 1]$ and can be interpreted as a percentage, not relative to the true value, but on the full scale of $[0, 1]$. We, therefore operationally define the margin of error used to identify convergence as

$$\text{margin of error} = \left| J_i^{\text{sample}} - J_i^{\text{true}} \right| \times 100 \tag{2}$$

To account for the stochastic nature of the samples, we created a one-sided, non-parametric prediction limit [41, 42] for the RVE size of each microstructure. The process described above for RVE determination was repeated for 19 different microstructures in each bin across the J-space, and the resulting RVEs were sorted in ascending order $\{\text{RVE}_1 ... \text{RVE}_{19}\}$. Without assuming anything about the nature of the resulting distribution, a 20th repetition would have probability $P = 1/20$, or a 5% chance, of having a value larger than RVE_{19}, and a probability $P = 19/20$, or 95% chance of having a value less than RVE_{19}. We therefore operationally define the RVE size for a particular microstructure to be equal to that of its corresponding RVE_{19} (as shown in Fig. 4).

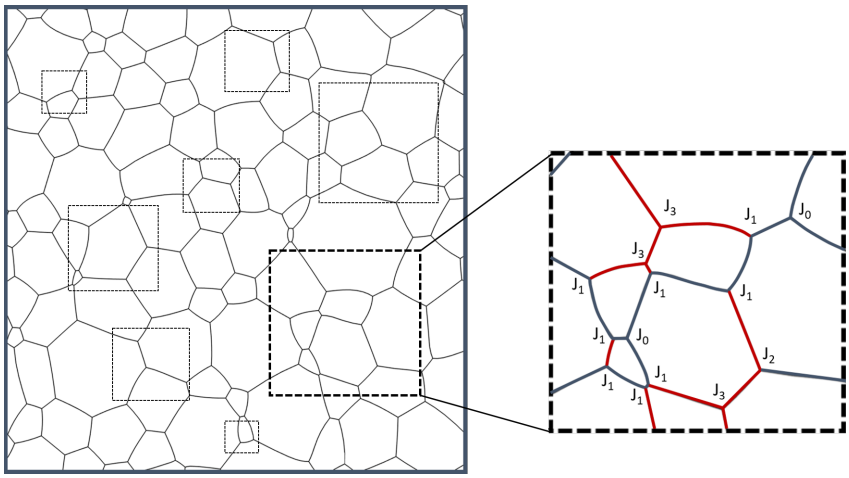

Figure 3: Samples of increasing size were taken at random locations throughout the microstructures. Each sample's GBN was analyzed and compared to the original GBN. This method was implemented for all microstructures and templates.

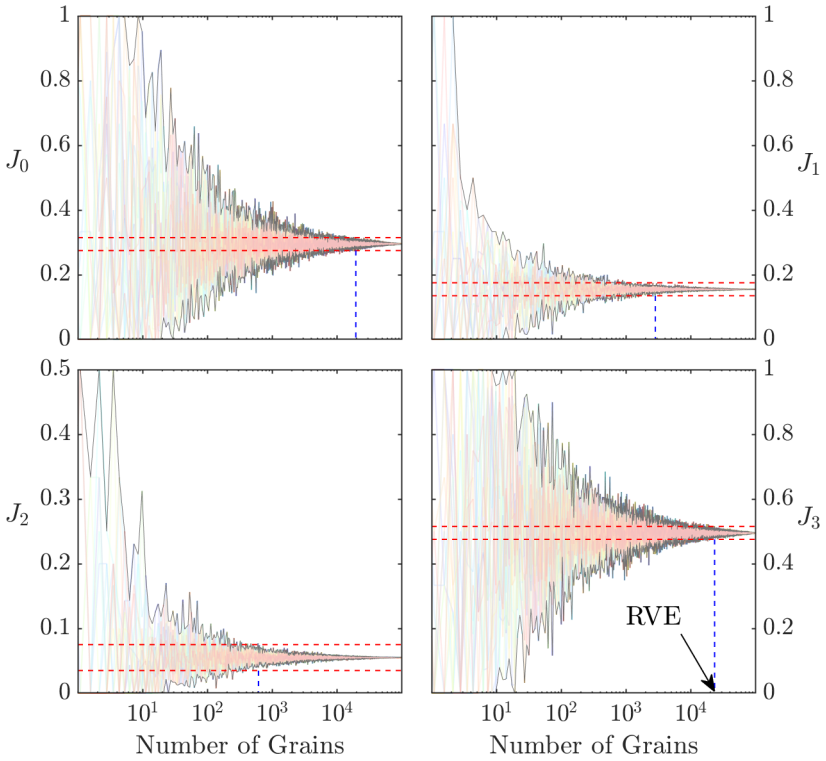

Figure 4: Illustration of the method used to define an RVE. Semitransparent colored lines are the TJ fractions of increasingly sized samples for the 19 different microstructures. The envelope of all 19 curves is shown in black. The red dashed lines correspond to the limits of the 2% error margin, and the dashed blue lines show where each TJ fraction converges. The highest number of grains at which one of the fractions converged was defined as the RVE.

The 19 different microstructures in each bin were generated via the Simulated Annealing procedure. For the grain growth templates a unique template was used for each of the 19 microstructures (the same 19 templates were used for every bin). The honeycomb templates have only a single configuration, so this universal honeycomb template was used 19 times for each bin.

RVE sizes for crystallographic texture were also determined using a similar method (see Fig. 5). A $3,000 \times 3,000$ grid of points, referred to as "point probes" in stereological parlance, was placed over the microstructure and each point probe was assigned the orientation of the grain in which it fell. This grid resembles the type of data acquired during a typical electron back-scatter diffraction (EBSD) scan, or the type of data collected during classical stereological examination of optical micrographs using reticles with superimposed point grids. Samples of increasing size were again taken at random locations in the microstructures. To avoid edge effects, samples were not taken within a distance of two average grain diameters from the edge of the sample. The space of grain orientations was discretized into 20 bins[1], and a discrete representation of the orientation distribution function (ODF) was calculated as the fraction of point probes within the sample whose orientations belonged to each bin (thus explicitly accounting for the effect and distribution of grain sizes), which we denote by ODF $= \{f_i \mid f_i = P_{P,i} \ \forall \ i \in [1, 20]\}$.This definition is intentionally similar to that used for the triple junction fractions to facilitate direct comparison of the results. We note also that it is one of the fundamental relations of stereology, $V_V = A_A = P_P$, that the point fraction is an unbiased estimate of both the area fraction and volume fraction [44–47] (note that this justifies the present approach, as well as the traditional use of EBSD point data to estimate an ODF). The size of the texture RVE was defined to be the smallest sample size for which the fraction of point probes (i.e. the probability of observing an orientation) in *all* of the bins matched that of the entire microstructure, to within the chosen margin of error. This procedure is essentially identical to that employed for the GBN, except that 20 orientation bins were employed instead of the 4 bins that defined the TJ types.

2.3. SVE Characterization

A similar method was used when characterizing SVE sets for each microstructure. An SVE set is composed of samples whose aggregate (either average or total) structure and/or properties are representative of the larger original microstructure. Thus, any sample size can be used to construct an SVE set if the cardinality of (i.e. the number of samples in) the set is large enough. Consequently, an RVE can be thought of as a special case of an SVE, whose corresponding set cardinality is equal to 1.

For reasons that will be explained in Section 3.5, we define the TJ fractions and texture of the SVE set according to

$$J_i = P_{P,i}^{\text{SVE}} = \frac{\sum_{k=1}^{K} N_{i,k}}{\sum_{k=1}^{K} N_k} \tag{3}$$

$$f_i = P_{P,i}^{\text{SVE}} = \frac{\sum_{k=1}^{K} N_{i,k}}{\sum_{k=1}^{K} N_k} \tag{4}$$

where $N_{i,k}$ denotes the number of points (either TJs or texture point probes, with the context distinguishing between the two in order to avoid overburdensome notation) of the i-th type observed within the k-th element of the SVE set, N_k denotes the total number of points (of all types) observed within the

[1] We experimented with a variety of discretizations, including the Freedman-Diaconis rule [43], which typically suggested around 45 bins. A higher number of bins (a higher resolution discretization) allows a more precise representation of the ODF, but at the cost of increasing the noise in the observed RVE trends. We selected a resolution of 20 bins in an effort to balance these competing objectives.

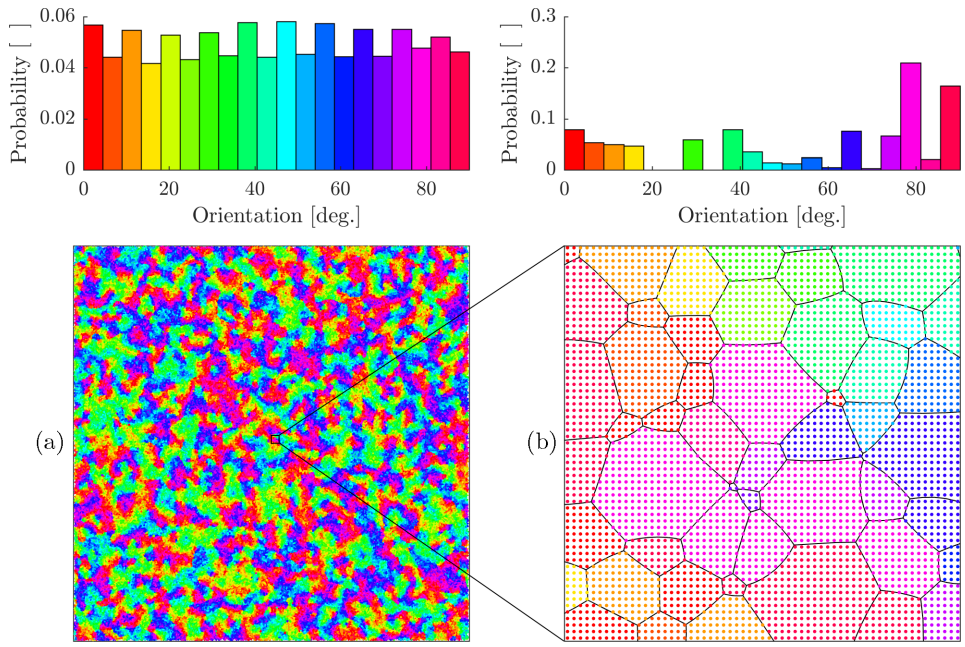

Figure 5: Illustration of the process for determining the RVE size for texture. In (a) the full microstructure is shown, together with its discrete orientation distribution function (above). In (b) a small sample taken from the center of the full microstructure is shown, together with its discrete orientation distribution function (above). In (b) the grid of point probes is clearly visible.

k-th element of the SVE set, and K denotes the SVE set cardinality. For each predetermined sample size considered, we defined the corresponding SVE set cardinality, K, as the number of samples for which the TJ fractions (or texture) of the entire set (Eqs. (3) and (4)) converged to those of the corresponding microstructure, using the same convergence criteria as described above for RVEs. Prediction upper-limits were again created for each bin in the J-space. The predetermined SVE sample sizes that were employed consisted of approximately 5, 10, 20, 50, 100, 500, and 1000 grains respectively.

The only significant methodological difference between the RVE and SVE calculation was in the placement of samples within the full microstructure. With increasing sample size the probability that some randomly placed samples overlap becomes non-negligible. For the RVEs, data from different samples is never combined and so the possibility of overlapping samples has no material impact on the results. For the SVEs, however, the data from different samples *is* combined and convergence depends on the union of a set of samples. If samples overlap, the union can be biased (e.g. a particular feature may be over-represented if it occurs in multiple samples) and in fact, in some cases, we observed that if randomly placed samples were used the set union may converge to the wrong values (texture or TJ fractions). Consequently, for SVE calculations, the microstructure was divided into a grid of non-overlapping samples, which were selected uniformly at random. This procedure also guarantees convergence because in the limit of using all of the non-overlapping samples, one has essentially used the entire microstructure. As shown in Section 3.2, SVE convergence occurred in all cases using only a small fraction of the available samples.

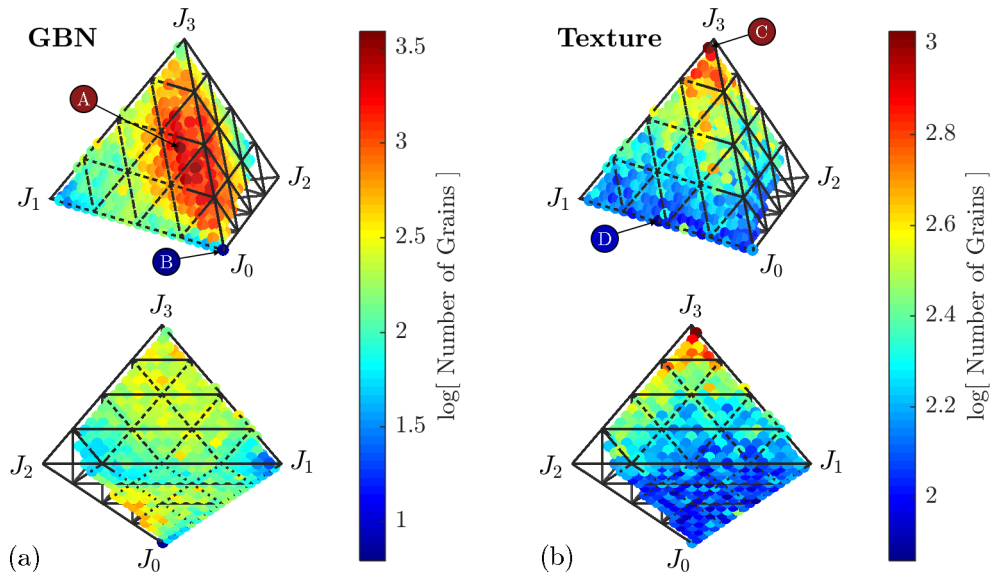

Figure 6: Grain growth polycrystal RVE results (with a 10% margin of error) for (left) the GBN and (right) crystallographic texture. The top and bottom rows show two different views of the J-space so that all faces of the tetrahedron are visible. Points labeled (A) and (B) indicate the largest and smallest GBN RVEs. Points labeled (C) and (D) indicate the largest and smallest texture RVEs. The corresponding microstructures are shown in Fig. 7. In the color legend, "log" refers to the base-10 logarithm.

3. Results and Discussion

3.1. RVE Sizes for Grain Boundary Networks and Texture

3.1.1. Trends over the J-Space

Figure 6(a) shows the GBN RVE results (with a 10% margin of error) for each bin in the J-space for the grain growth templates. As expected, microstructures in bins near the vertices of the J-space have low GBN RVE sizes, especially near the J_0 and J_1 vertices. These microstructures consist predominantly of one type of TJ, so it is easier for a smaller random sample to be representative. Away from the vertices, there is a clear trend of increasing RVE sizes toward the J_0–J_3 edge, where microstructures are made up of mostly type 0 and type 3 TJs. This trend can be explained by considering the feasible microstructural configurations that inhabit the J_0–J_3 edge. Since type 0 and type 3 TJs cannot share a GB, it is only possible to approach the J_0–J_3 edge in the limit of infinite-sized microstructures [48] having TJ types segregated in such a way that the fraction of TJs lying on the interface between type 0 and type 3 regions (themselves being type 1 or type 2 TJs) asymptotically vanishes with increasing microstructure size. Consequently, convergence would require the RVE to approach the (infinite) size of the full microstructure.

For crystallographic texture (Fig. 6(b)), both the trends and sizes of RVEs across the J-space are noticeably different. The texture RVEs increase in size towards the J_3 corner, and are smallest across the J_0–J_1–J_2 plane. This trend is somewhat counterintuitive since an obvious example of a microstructure having $J_3 = 1$ would be a single crystal, which would have an extremely small RVE. The explanation, which will be given in Section 3.1.2, lies in consideration of the configurational entropy in the microstructure.

3.1.2. Microstructures of the Largest and Smallest RVEs

Figure 7 shows the microstructures corresponding to the largest and smallest RVEs for both GBNs and texture (the corresponding locations in the J-space are indicated in Fig. 6).

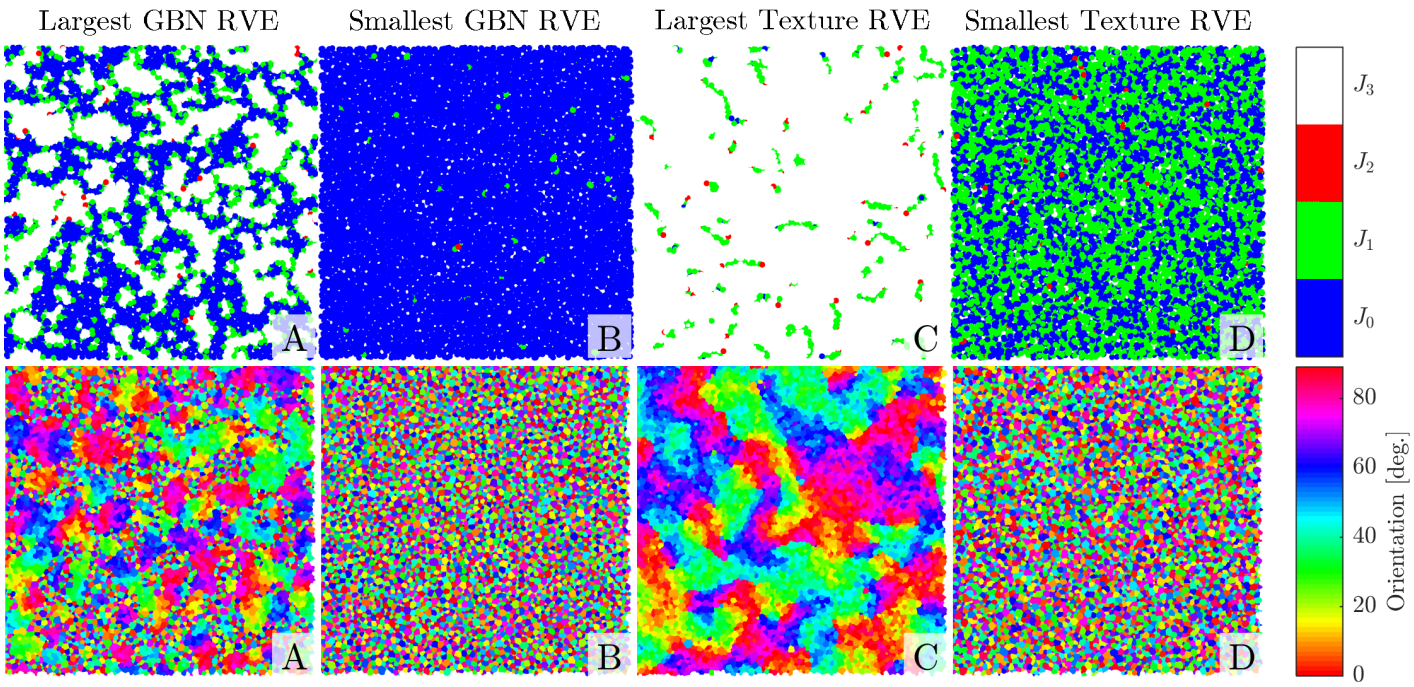

Figure 7: Microstructures of the largest and smallest RVEs for GBN and texture, corresponding to the points indicated in Fig. 6 (shown at 4× magnification—each frame shows about 6,250 grains, which represents a view of about 6.25% of the full respective microstructure). In the top row only the TJs are plotted, and they are colored by their TJ type. In the bottom row, the grains are colored by their crystallographic orientation.

The microstructure of the largest GBN RVE (3,887 grains) has TJs that appear phase-separated into pure J_0 and pure J_3 phases with J_1 and J_2 type TJs at the interface. To achieve this, the texture also phase-separated into a phase having similar orientations internally (and therefore having nearly all low-angle GBs, which results in the pure J_3 TJ phase in the same region) and a phase having dissimilar orientations internally (and therefore having nearly all high-angle GBs, which results in the pure J_0 TJ phase in the same region). The texture RVE for this bin in the J-space is of an intermediate size (305 grains), relative to other texture RVEs, and is more than an order of magnitude smaller than the corresponding GBN RVE.

The microstructure of the smallest GBN RVE (7 grains) has a GBN consisting of nearly all J_0 type TJs. As shown in Fig. 8, the texture for this microstructure (in fact for all A-C) is uniform. The texture RVE for this bin is larger than the GBN RVE (150 grains), but is small on the scale of other texture RVEs.

As mentioned previously, the largest texture RVE (1,065 grains) occurs near the J_3 corner, which is counterintuitive because a simple example of a microstructure with all type 3 TJs is a single crystal, which would have a very small RVE (both for texture and GBN). However, a single crystal is a state with extremely low configurational entropy. Consequently, the Monte Carlo procedure used to generate these microstructures has negligible probability of encountering a single crystal state. The number of polycrystalline configurations that have nearly all type 3 TJs is much larger, and consequently the configurational entropy for an equivalent polycrystalline state is much greater and these are the states that the Monte Carlo procedure will therefore encounter. It is also worth recalling that the RVE sizes presented are the 95% prediction upper limit, which is defined as the largest RVE of 19 microstructural realization in a given bin. This means that even if a single crystal state had been included in the set of 19 microstructures in this bin, it would not change the RVE size of this bin. To achieve a polycrystalline

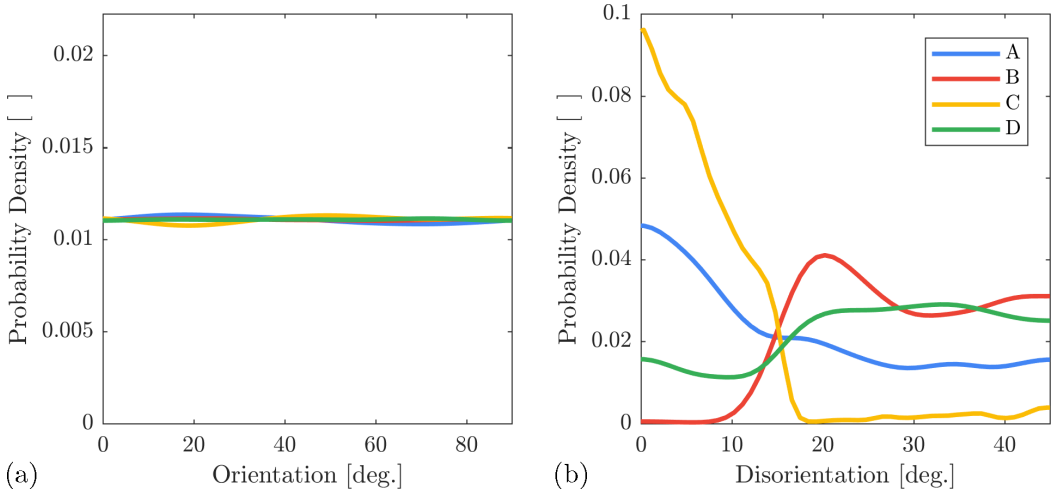

Figure 8: (a) Orientation distribution functions (ODFs) and (b) GB disorientation distribution functions for each of the microstructures shown in Fig. 7.

microstructural configuration with nearly all type 3 TJs, Fig. 7 shows that this microstructure consists of clusters of similar orientation (essentially the microstructure has tried to locally become a single crystal, and this is one of the many polycrystalline local minima in the configuration space). While the ODF for this texture is uniform like the others (see Fig. 8(a)), there are clearly much longer-range spatial correlations than with the other textures, which leads to the much larger texture RVE even though the global macro-texture is the same. Evidence of this spatial correlation also appears in the form of the strong peak that is visible in the disorientation angle distribution for small disorientation angles (Fig. 8(b)). The GBN of this microstructure consists of a matrix of J_3 TJs containing a dilute concentration of stringy chains of J_1 TJs that terminate in J_0 and J_2 TJs. The GBN RVE for this bin is intermediate in size (141 grains) compared to other GBN RVEs and is nearly an order of magnitude smaller than the corresponding texture RVE.

The microstructure of the smallest texture RVE (73 grains) has a texture that visually appears very similar to that of the smallest GBN RVE (microstructure B in Fig. 7) and their ODFs are essentially indistinguishable. Both of these microstructures inhabit the J_0–J_1–J_2 plane, and, as shown in Fig. 6(b), all of the microstructures occupying that plane have very low texture RVE sizes.

Although the ODFs are similar, the TJ characteristics across the J_0–J_1–J_2 plane vary significantly as do the GBN RVE sizes. Consideration of the disorientation angle distribution (Fig. 8(b)) reveals that the spatial correlations in microstructure D are much weaker than in microstructure B, as the disorientation angle distribution is much more uniform for microstructure D than for microstructure B. The GBN of this microstructure consists of a nearly 50/50 mixture of type 0 and type 1 TJs. As observed by Frary et. al [30], this kind of TJ distribution leads to a GBN configuration that prefers mixing rather than phase-separation, which is what we also observe. This also explains the stark contrast between the GBN of microstructure D and microstructure A, both visually and quantitatively. Both consist of a 50/50 mixture of two types of TJs. However, in microstructure A these were type 0 and type 3 TJs, which *cannot* share a GB—and this is the reason for the phase-separation behavior (they are essentially "immiscible" TJ types)—whereas in microstructure D these are type 1 and type 0 TJs, which *can* share a GB—and this is the reason for the mixing behavior (they are highly miscible TJ types). This mixing behavior is the reason that the GBN RVE for this bin (200 grains) is much smaller than that of microstructure A.

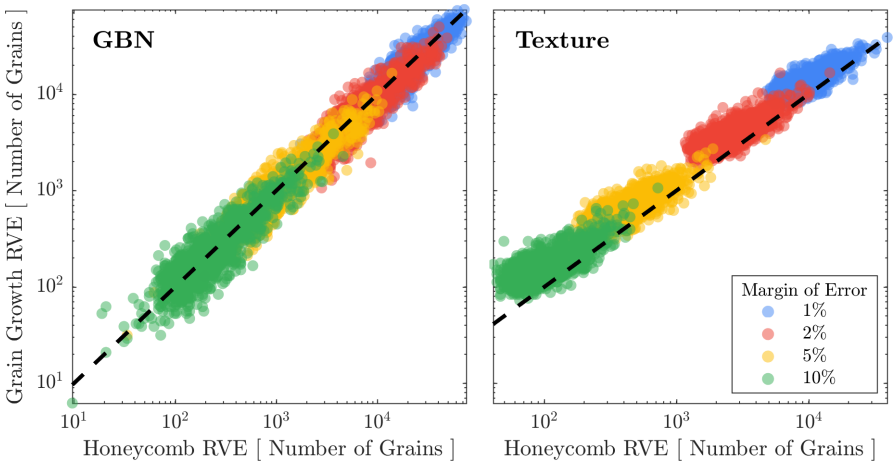

Figure 9: Comparison of RVE sizes found for the grain growth templates to those for the honeycomb templates, for both GBN and texture. The dashed line represents a 1:1 correspondence.

3.1.3. Comparison of Grain Growth and Honeycomb Templates

Figure 9 shows the RVE sizes obtained using the grain growth templates compared to those found for the idealized honeycomb templates for both GBN and texture. For GBNs the RVE sizes are comparable, though the grain growth templates had on average a small bias for being smaller than the corresponding honeycomb templates (between 51%–56%—depending on the margin of error—of the grain growth templates had smaller RVEs than the corresponding honeycomb templates).

In contrast, for texture 94%–97% of the grain growth templates had larger RVEs than their honeycomb counterparts, and between 39%–57% of the grain growth templates are at least 50% bigger (i.e. it is both the frequency and magnitude that are significant). This suggests that—at least when TJ fractions defined by the low-angle/high-angle definition of special vs. general GBs are the relevant microstructural feature—the commonly employed honeycomb idealization may be a satisfactory approximation, but when texture is a relevant microstructural feature, this idealization is likely unsatisfactory.

The reason that the texture is more significantly affected by this idealization than the GBN can probably be attributed to the higher dispersion in the grain size distribution (ratio of standard deviation to mean of 0.7672) than the distribution of the number of TJs per grain for the grain growth templates (ratio of standard deviation to mean of 0.2108), while maintaining an almost identical average grain size and average number of TJs per grain as the honeycomb templates. Stated another way, the more realistic grain growth templates are topologically very similar to the idealized honeycomb templates, but geometrically quite distinct. Consequently, for the remainder of this work, we focus on the results for the grain growth templates.

3.1.4. Comparison of GBN and Texture RVE Sizes

Figure 10(a) shows the cumulative distribution function (CDF) of RVE sizes over the J-space for both GBN and texture for all margins of error. This view allows one to select an RVE size depending on the required accuracy (margin of error) and precision (how much of the distribution of RVE sizes over the J-space it will be representative of—or in other words, if the TJ distribution is not known *a priori*, how conservative one desires to be). For example, if a 10% margin of error is desired, an RVE size of 441 grains would be expected to be sufficient for 80% of the J-space for the GBN, or 231 grains for texture.

One important observation from Fig. 10(a) is that, while two of the four examples shown in Fig. 7 had larger RVEs for texture than for the GBN, across the full J-space most bins (between 63%–82% as

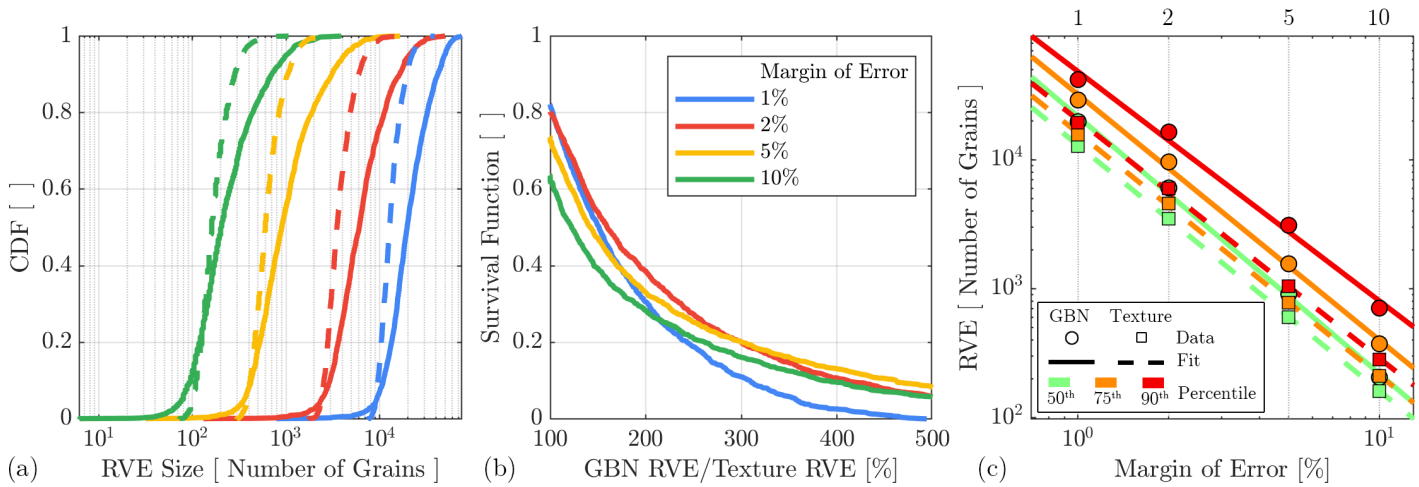

Figure 10: (a) Cumulative distribution function (CDF) of RVE sizes over the J-space for both GBN and texture, which shows the fraction of bins in the J-space with an RVE size less than or equal to a given value. Solid lines are for GBN, dashed lines are for texture, and colors indicate the margin of error. (b) Survival function of the ratio of GBN RVE size to texture RVE size, which shows the fraction of bins in the J-space for which the GBN RVE is *at least* a given percentage larger than the corresponding texture RVE (this simultaneously quantifies how often GBN RVEs are larger than texture RVEs and by how much). The horizontal limits are restricted to 100%–500% for the sake of visual clarity. There is only one line style because the data represents the *ratio* of GBN and texture RVE sizes. (c) P^{th} percentile RVE size as a function of margin of error, for $P \in \{50, 75, 90\}$. Both axes are logarithmically scaled, but the horizontal axis limits cover a single decade. The median is the 50th percentile (green), higher percentile RVE sizes are also shown to enable users to select a more conservative size if desired. The GBN 50th percentile markers are difficult to see as they fall almost exactly underneath the Texture 90th percentile markers.

indicated by the vertical intercept in Fig. 10(b)) have a larger RVE for the GBN than for texture. To quantify both how often the GBN RVEs are larger than the texture RVEs *and* by how much, Fig. 10(b) shows the survival function of the ratio of GBN RVE size to texture RVE size. This data suggests that the trend of GBN RVE size being larger than texture RVE size is both general and of significant magnitude. For example, between 11%–20% of the J-space have GBN RVEs that are *at least* 3 times as large as the corresponding texture RVE, 28%–39% are at least twice as large, and nearly half of the space (39%–54% of the bins) have GBN RVEs that are at least 50% larger than the corresponding texture RVE. This suggests that the length-scale of heterogeneity (which is effectively what the size of an RVE is dictated by) for GBNs is naturally significantly larger than for texture. This has important implications relative to materials science research, as it suggests that the use of RVE sizes that are appropriate for texture—which have been studied in the literature—will generally be quite inadequate for the study of GBNs.

We note in passing that PDFs corresponding to the CDFs shown in Fig. 10(a) are approximately log-normal, but with slightly heavier tails.

In Section 3.1.1 we described the trends in RVE size over the J-space. However, in the design phase of an experimental or computational research effort, one may not know *a priori* what type of TJ fractions to expect in the samples that will be employed, but it will often be critical to prudently choose an appropriate sample size so that the results obtained can be general rather than specific to the idiosyncrasies of a particular sample. A reasonable starting place could be the median (50th percentile) RVE size across the entire J-space. Figure 10(c) shows how the Pth percentile RVE size varies with margin of error for both GBNs and texture, for $P \in \{50, 75, 90\}$. The observed relationship is well approximated by a power-law (note the approximate linearity on the log-log plot shown in Fig. 10(c)). Several notable observations can be made from Figure 10(c).

First, the power-law dependence of RVE size on margin of error implies that relatively small increases in accuracy (i.e. reducing the margin of error) can require significant increases in sample size. Thus accuracy, in this case, is expensive and results in an inevitable trade-off that must be made, highlighting the importance of quantifying RVE size so that an optimal trade-off can be achieved.

Second, as can also be seen in Figs. 6 and 10(a), the median RVEs for GBNs are larger than for texture, with the median GBN RVE for the grain growth templates being as much as 72% larger than the median texture RVE (for a 2% margin of error). However, at larger margins of error the difference is somewhat diminished, so that, as a useful heuristic, if 10% error is acceptable a conveniently small RVE (about 200 grains) may be used for both texture and GBN sensitive applications. Table 1 lists the numerical values for the median and maximum RVE sizes for GBNs and texture, for both the grain growth and honeycomb templates. It is worth noting that the maximum RVE sizes for GBNs (for the grain growth templates) are between 3.8–18.9 times as large as the median. Thus, the cost of being extremely conservative (using the maximum RVE size over the J-space) is very high. In contrast, for texture (again for the grain growth templates) the maximum RVE sizes are between 3.0–6.6 times as large as the median: still a large increase, but this shows that the variation in RVE size for texture is not as large as for GBNs.

Table 1: GBN and texture RVE sizes for the honeycomb and grain-growth templates. The maximum and median RVEs spanning the J-space are listed for each respective margin of error. Values are given in units of number of grains.

Margin of Error	Honeycomb				Grain Growth			
	GBN RVE		Texture RVE		GBN RVE		Texture RVE	
	Max	Median	Max	Median	Max	Median	Max	Median
1%	75,554	19,490	39,259	8,701	75,816	19,734	38,891	12,780
2%	48,701	5,920	14,440	2,323	50,184	6,041	16,708	3,508
5%	13,898	900	4,715	387	16,547	908	3,386	602
10%	4,575	210	723	99	3,887	206	1,065	161

3.2. Cardinality of SVE sets for GBNs and Texture

3.2.1. Trends over the J-Space

Figure 11 shows the SVE cardinality results using a 10 grain sample size (with a 10% margin of error) for each bin in the J-space for the grain growth templates. As expected, the trends over the J-space are similar to those for RVE sizes, though with slightly more noise in the case of texture.

Table 2 provides the numerical values of the median and maximum SVE cardinalities for each sample size for a 1% and 10% margin of error.

3.2.2. Comparison of SVE Cardinality for GBNs and Texture

Figure 12(a)–(b) show the CDFs of SVE cardinality as a function of SVE sample size for both GBNs and texture. As would be expected, as SVE sample size increases, the number of samples required decreases. We find that SVE cardinality scales with the SVE sample size as a power law (note the linearity of the contour lines on this doubly logarithmic plot), resulting in a dramatic increase in the number of required samples as their size decreases. This power law breaks down for larger margins of error at sufficiently large sample sizes (note the bending of the 10% margin of error contours above a sample size of about 100 grains and the eventual saturation for 1000 grains) as the cardinality is integer valued and cannot be less than 1.

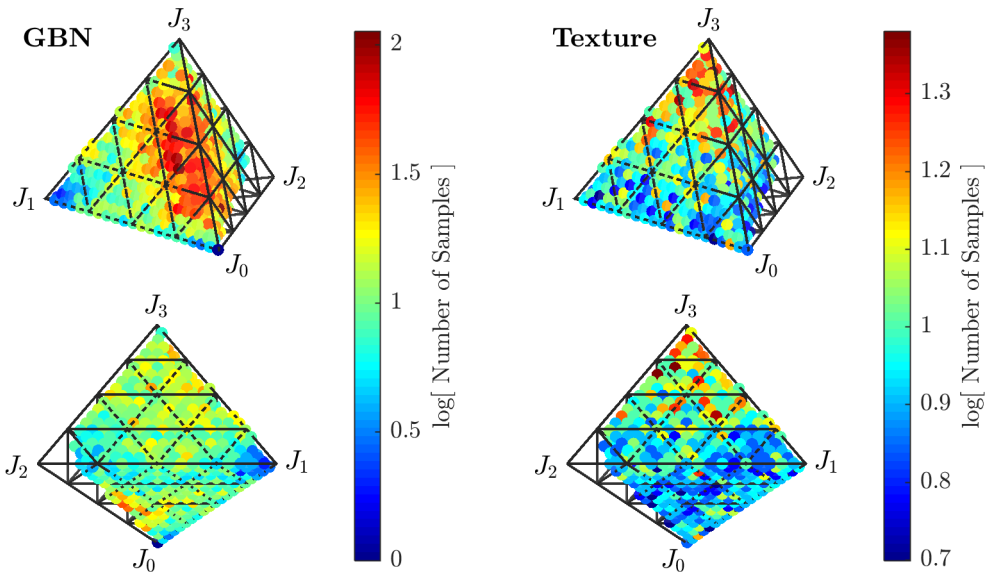

Figure 11: The cardinality of an SVE set, where the size of each sample is equivalent to approximately 10 grains, for grain growth polycrystal templates (with a 10% margin of error) for (left) the GBN and (right) crystallographic texture. The top and bottom rows show two different views of the J-space so that all faces of the tetrahedron are visible. In the color legend, "log" refers to the base-10 logarithm.

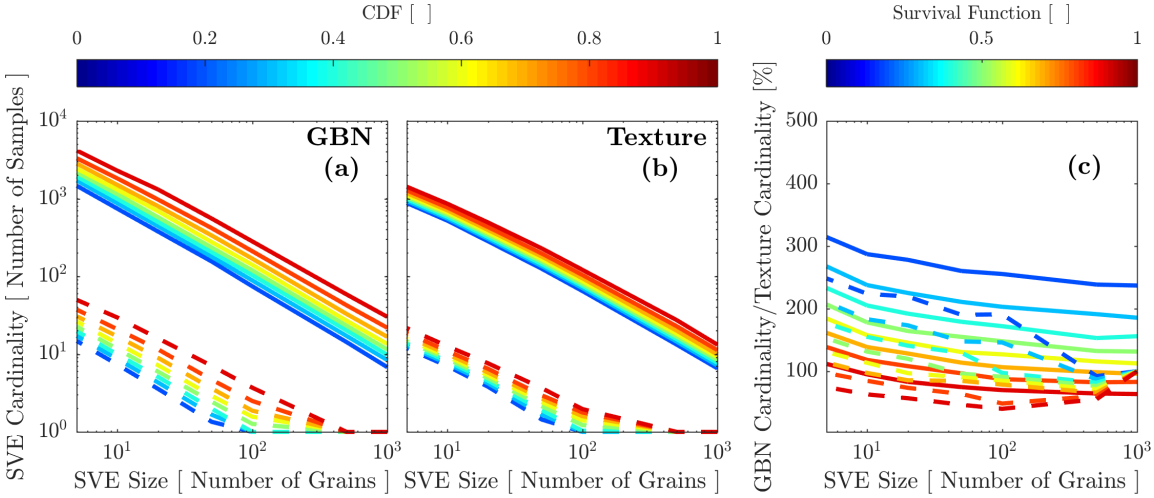

Figure 12: Cumulative distribution function (CDF) of SVE cardinality over the J-space for both (a) GBNs and (b) texture as a function of SVE sample size. The solid contour lines represent the CDF for a 1% margin of error, and the dashed contours show the CDF for a 10% margin of error. (c) Survival function of the ratio of GBN SVE cardinality to Texture SVE cardinality. Again, the solid contour lines are for a 1% margin of error, and the dashed contours are for a 10% margin of error.

Table 2: GBN and texture SVE cardinality for 1% and 10% margins of error for grain growth polycrystal templates.

SVE Size [# of grains]	1% Error				10% Error			
	GBN Cardinality		Texture Cardinality		GBN Cardinality		Texture Cardinality	
	Max	Median	Max	Median	Max	Median	Max	Median
5	8,577	2,180	2,260	1,045	142	23	41	15
10	4,586	1,141	1,590	624	113	12	24	9
20	2,912	579	955	344	60	6	17	5
50	1,296	236	481	155	36	3	10	3
100	712	120	417	81	17	2	6	2
500	124	24	67	17	5	1	2	1
1000	68	12	33	9	3	1	1	1

As the margin of error increases, fewer samples are required (note the downward shift of the contours in Fig. 12(a)–(b) from 1% margin of error to 10% margin of error). As with the RVE sizes, we also observe that the SVE cardinality scales as a power law with margin of error.

Again, to quantify how often the cardinality of the GBN SVEs is larger than for the texture SVEs *and* by how much, Fig. 12(c) shows the survival function of the ratio of GBN SVE cardinality to texture SVE cardinality, for each SVE size. This data suggests that GBN SVE cardinality is generally larger than texture SVE cardinality, and that this trend is only weakly affected by SVE sample size (note the nearly flat contours, particularly for the 1% margin of error). However, at larger margins of error and the largest sample sizes, the cardinality of GBN and texture SVEs is essentially equal (note how the 10% margin of error contours converge for SVEs with 1000 grain sample sizes). As an example of the frequency and magnitude of the difference between GBN and texture SVE cardinalities, for SVE sets with a 10 grain (100 grain) sample size across all margins of error, between 11%–20% (6%–18%) of the J-space have GBN SVE cardinalities that are *at least* 3 times as large as the corresponding texture SVE cardinalities, 24%–43% (13%–34%) are at least twice as large, and 41%–63% (28%–49%) of the bins in the J-space have GBN SVE cardinalities that are at least 50% larger than the corresponding texture SVE cardinalities. For very small (5 grain) SVE sample sizes the cardinality ratio is slightly higher, and for very large (1000 grain) SVE sample sizes the cardinality ratio is lower. The frequency and magnitude of the GBN to texture SVE cardinality ratio is comparable to that of the GBN to texture RVE size ratio (see Section 3.1.4 and Fig. 10).

3.3. Comparison of RVEs and SVEs

The data collected here for both RVEs and SVEs allows us to make a quantitative comparison of the efficiency of using RVEs vs. SVEs for GBNs and texture. To do this, we compare the total number of grains required to define an RVE to the total number of grains required for an SVE set—which is the product of SVE sample size and SVE cardinality—for the same bin in the J-space. This allows us to see the influence, if any, of SVE sample size. In this context, to determine under what circumstances it is more beneficial to use an RVE or an SVE set we have simply to answer the question, "Which of the two requires more grains?" If more grains are required for an RVE than for the corresponding SVE set then it is more advantageous (efficient) to use an SVE set.

Figure 13 shows the survival functions for the ratio of the required number of grains for an RVE to the required number of grains for an SVE set, for GBNs and texture. Several observations are notable.

First, when high accuracy is required (1% margin of error), it is almost *always* more efficient to

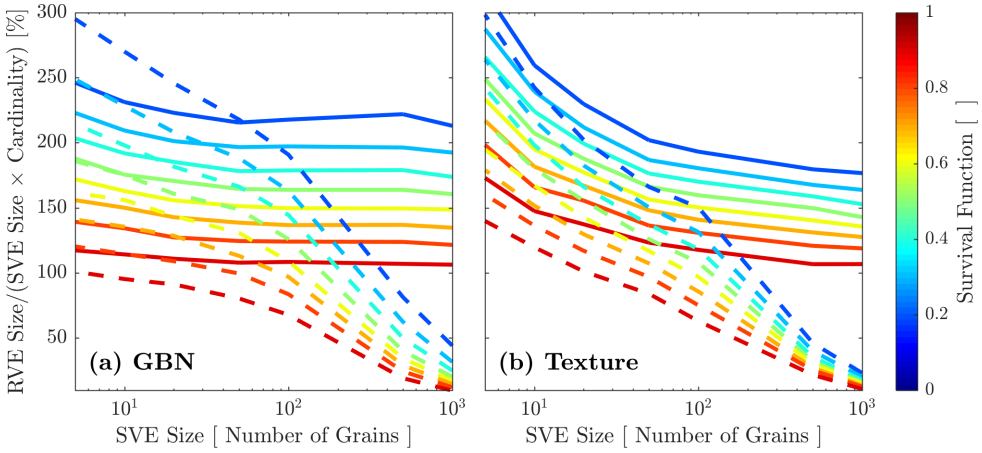

Figure 13: Survival function for the ratio of RVE Size to the product of SVE size and cardinality for (a) GBNs and (b) texture as a function of SVE sample size. Again, the solid contours are for a 1% margin of error, and the dashed contours are for a 10% margin of error.

use an SVE set (for GBNs, between 92%–96% of the bins have an RVE that requires more grains than the corresponding SVE set; for texture, the figure is 94%–100% depending on the SVE sample size). For GBNs, this is essentially independent of SVE sample size (note the horizontal contours for the 1% margin of error in Fig. 13(a)), whereas for texture (Fig. 13(b)), the efficiency of using an SVE compared to an RVE grows as the SVE sample size decreases.

When a larger margin of error (10%) is permissible, the situation is quite different and the efficiency of an SVE over an RVE depends strongly on the selected SVE sample size. For small sample sizes the result is not significantly changed from the high accuracy (1% margin of error) case. However, for larger sample sizes SVE sets begin to require significantly more grains in aggregate than the corresponding RVE. It is important to note that this does not mean that an RVE becomes preferable to an SVE set for a 10% margin of error. Rather, recall that the number of grains in the RVE is fixed, it is the number of grains in the SVE set that is changing with SVE sample size; thus, the observed trend indicates only that using *large* SVE sample sizes becomes undesirable. There is always, apparently, a small enough SVE sample size for which an SVE set will require fewer grains than the corresponding RVE over the vast majority of the J-space.

It may be surprising that the ratio of the required number of grains in an RVE to the required number of grains in an SVE set deviates from unity (or 100%) at all. However, we note that the grains sampled in an RVE are in a contiguous region of the microstructure, whereas an SVE set is composed of samples from many non-contiguous regions of the microstructure. As a result, the diameter of an SVE set will be strictly greater than or equal to the diameter of an RVE containing the same number of grains (assuming the SVE elements are non-overlapping, as enforced in the present work). Thus, the SVE set interrogates larger microstructural length-scales for the same number of grains, the corollary is that an SVE set requires fewer grains to characterize the same microstructural length scale present in an RVE. We suggest that this is the reason that SVE sets are more efficient than RVEs.

We note in passing that the fact that large SVEs can be undesirable is consistent with this hypothesis because the diameter of a set of large SVEs may be much larger than the length-scale of heterogeneity of the microstructure, meaning that more of the microstructure is measured than is necessary without any additional gain in information (i.e. there are diminishing and eventually negative returns as the size of SVE samples increase), so the potential efficiency of the non-contiguous sampling strategy intrinsic to SVE sets is not well exploited by large SVEs.

The number of grains required is a measure of the *size* of the problem to be solved (whether via calculations from computer simulations, or experimental characterization). There is another important consideration related to the efficiency of SVE sets vs. RVEs: the potential for parallelization. The use of SVE sets presents what is referred to as an "embarassingly" or "pleasingly" parallel problem: every sample in the set can be simulated/characterized independently of all of the others. Parallelization can also be used for RVEs, but the problem is a distributed computing problem that requires communication overhead. The potential for massive parallelization that SVEs provide is a significant additional benefit for computational work. For experimental characterization this additional benefit is not likely to be as large, because the simultaneous use of multiple experimental apparatuses (e.g. property measurement equipment, or electron microscopes) to parallelize the measurement/characterization task is likely to be limited to at most 2–3 duplicate pieces of equipment. Consequently, experimental resource constraints, and the additional setup cost of each experiment, may actually justify the globally sub-optimal use of an RVE instead of an SVE set in some experimental contexts. In either case, the findings presented here may facilitate the strategic decision making process in the presence of these trade-offs, and in some cases the required RVE size may be too large to be practical even for an experimental measurement, in which case the results presented here can guide the researcher to select the number of samples required for the sample size that is practical in a particular application (e.g. see Table 2).

3.4. Comparison to Experiment

The present work represents the first time that RVEs and SVEs have been determined for GBNs. However, for texture, there are numerous studies in which RVEs have been determined, allowing us to compare the values obtained here to those published in the literature. Methods for determination of RVE sizes for texture vary widely and include convergence of the ODF or disorientation distribution function (DDF) [27, 49, 50] and indirectly analyzing texture by instead determining convergence of measured properties (e.g. elasticity or fatigue) [51–53]. Convergence criteria (how one defines the point at which a sample becomes "representative") also vary between studies, including minimizing the difference between EBSD and X-ray diffraction ODFs [54], minimizing deviation from known values (of structure or properties) [50], and minimizing standard deviation from repeated measurements/simulations [3, 52].

Although the methods are diverse, texture RVE sizes[2] determined from experimental measurements are in the range of $10^{1.4}$ grains to $10^{4.0}$ grains [27, 49, 50, 54, 55], and texture RVE sizes determined from simulation are in the range of $10^{1.3}$ grains to $10^{2.3}$ grains [51–53, 56–58]. In spite of the use of a wide range of methods and convergence criteria in the literature, Table 3 shows that the texture RVE sizes found in the present work span a similar range as those found in the literature and are therefore consistent with prior work, and with experimentally determined RVE sizes.

3.5. Predictions for Three-Dimensional Microstructures

While the microstructures considered here were two-dimensional, the results may also be adapted for fully three-dimensional microstructures under a broad range of conditions via stereological methods. To extract three-dimensional RVE sizes and SVE cardinalities from the two-dimensional RVEs and SVEs we must first establish the relationship between the two-dimensional microstructural characteristics measured here (TJ fractions and texture) and their three-dimensional counterparts, and then we must

[2]Most of the RVE sizes quoted in the literature represent the number of grains in a 3D volume, which we denote by N_{3D}. To compare these values with the RVE sizes of the present work, which represent the number of grains in 2D microstructures, and which we denote by N_{2D}, we have converted any literature values expressed as N_{3D} to their equivalent N_{2D} by means of Eq. (14). However, regardless of whether or not this conversion is applied, the range of values in the present work compares favorably with the range of values reported in the literature.

Table 3: Range of grain growth RVE sizes for GBNs and Texture found in the present work for all margins of error.

Margin of Error	GBN RVE		Texture RVE	
	Min	Max	Min	Max
1%	$10^{2.9}$	$10^{4.9}$	$10^{3.9}$	$10^{4.6}$
2%	$10^{2.1}$	$10^{4.7}$	$10^{3.2}$	$10^{4.2}$
5%	$10^{1.5}$	$10^{4.2}$	$10^{2.5}$	$10^{3.5}$
10%	$10^{0.8}$	$10^{3.6}$	$10^{1.9}$	$10^{3.0}$

establish the relationship between the number of grains (our defined unit of RVE size) observed in a plane section and the number of grains in a corresponding three-dimensional volume.

The fundamental relations of stereology allow quantitative measurement of certain three-dimensional microstructural features from two-dimensional sections. In particular, an unbiased estimate of the total length of triple junctions per unit volume (L_V) in a three-dimensional microstructure can be determined from the expected value of the number of triple junction points per unit area (P_A) that appear in an ensemble (i.e. an SVE set) of two-dimensional samples according to [45]:

$$L_V = 2\,\langle P_A \rangle \tag{5}$$

where $\langle \cdot \rangle$ denotes the expected value (ensemble average). As we are concerned with distinguishing between different types of triple junctions, we can employ Eq. (5) to derive a relationship between the two-dimensional triple-junction fractions (which are point fractions) used in this work and their three-dimensional counterparts (which are length fractions):

$$J_i^{3D} = \frac{L_{V,i}}{L_V} = \frac{2\,\langle P_{A,i} \rangle}{2\,\langle P_A \rangle} = \frac{\frac{1}{K}\sum_{k=1}^{K} N_{i,k}/A}{\frac{1}{K}\sum_{k=1}^{K} N_k/A} = \frac{\sum_{k=1}^{K} N_{i,k}}{\sum_{k=1}^{K} N_k} \tag{6}$$

where the subscript i distinguishes the respective length-per-unit-volume, number of points-per-unit-area, and number of points of the i-th TJ type from the corresponding total values, and where we have made use of the fact that all K elements of a fixed-size SVE set—as defined in the present work—have equal areas. Comparison of Eq. (6) with Eq. (3) shows that

$$J_i^{3D} = J_i^{2D} \tag{7}$$

indicating that the triple-junction number fractions measured from 2D SVE sets are unbiased estimators of the triple-junction length fractions in the corresponding 3D microstructure. Although straightforward to derive, we are not aware of this relationship having been derived previously in the literature. It is worth noting that defining the two-dimensional TJ fractions according to the reasonable alternative, $J_i^{2D} = \langle N_i/N \rangle$, would not exhibit this important property. It is therefore recommended to the community that TJ fractions for 2D SVEs be defined according to Eq. (3), as done in the present work, so that comparison to 3D microstructures can be made.

For crystallographic texture, we can derive a similar relation relating the three dimensional volume fractions of each orientation bin (f_i^{3D}) to the point fractions measured on two-dimensional planes (f_i^{2D}), which is one of the most ubiquitous of all metallurgical stereological measurements:

$$f_i^{3D} = \frac{V_i}{V} = V_{V,i} = \langle P_{P,i} \rangle = \frac{1}{K}\sum_{k=1}^{K} \frac{N_{i,k}}{N_k} = \frac{\sum_{k=1}^{K} N_{i,k}}{\sum_{k=1}^{K} N_k} \tag{8}$$

where the stereological notation $V_{V,i}$ denotes the volume fraction of the i-th orientation bin, $P_{P,i}$ denotes the point fraction of the i-th orientation bin, and we have made use of (i) the fundamental sterological identity $V_V = \langle P_P \rangle$ [45–47], and (ii) the fact that all K elements of a fixed-size SVE set have an equal number of point probes (i.e. all of the N_k are equal, and so $\sum_{k=1}^{K} N_k = KN_k$). Comparison of Eq. (8) with Eq. (4) shows that

$$f_i^{3D} = f_i^{2D} \tag{9}$$

indicating that textures measured from 2D SVE sets are unbiased estimators of the textures in the corresponding 3D microstructure. Obviously, Eqs. (7) and (9) hold for RVEs also, which are just SVE sets whose cardinality is equal to unity. Because Eqs. (7) and (9) apply to both the macroscopic microstructure as well as the smaller samples which are used to determine the RVEs and SVEs, it follows that convergence of the 2D samples to the macroscopic 2D microstructural statistics coincides with convergence of the equivalent 3D samples to the macroscopic 3D microstructural statistics.

To convert the sizes of 2D RVEs and SVEs to their corresponding sizes in 3D, all that remains is to determine the relationship between the number of grains in a 3D volume and the number of grains observed on 2D planes that intersect that volume. Due to the fact that grains are not always convex, an exact analytical solution to this problem is not currently available. However, analytical solutions can be obtained for some of the space-filling convex tessellations commonly employed to model polycrystalline microstructures. For convex objects we have [44–47]

$$N_V = \langle N_A \rangle / \langle D \rangle \tag{10}$$

where N_A is the number of grains per unit area, N_V is the number of grains per unit volume, and $\langle D \rangle$ is the mean caliper diameter of the grains (sometimes called the mean breadth, and alternatively denoted $\langle B_3 \rangle$). For a 3D Poisson-Voronoi tessellation (sometimes used to model polycrystalline microstructures) an analytical expression for $\langle D \rangle$ can be obtained, yielding the relationship [46]

$$N_V = C \langle N_A \rangle^{3/2} \tag{11}$$

where $C = \frac{15\sqrt{5}}{4}\pi^{-5/2}\left[\Gamma\left(\frac{4}{3}\right)\right]^{-3/2}$. Because all elements of a fixed-size SVE have equal area, the ensemble average of N_A over an SVE set is given by $\langle N_A \rangle = \langle N_{2D} \rangle / A$, where N_{2D} is the number of grains observed in a 2D plane of area A. Substituting this into Eq. (11), and considering a cube-shaped volume of side length L, we then have

$$N_{3D} = N_V L^3 = C\left(\frac{\langle N_{2D} \rangle}{L^2}\right)^{3/2} L^3 = C \langle N_{2D} \rangle^{3/2} \tag{12}$$

or

$$N_{3D} \approx 0.5680 \langle N_{2D} \rangle^{3/2} \tag{13}$$

Although an analytical expression is not available for the non-convex grains that exist in real polycrystals, a numerical approximation can be obtained. Using DREAM.3D [59], we simulated 42 three-dimensional polycrystals with equiaxed grains having N_{3D} ranging from about 18 grains to 72,929 grains and determined N_{2D} (which ranged from about 5 grains to about 1663 grains) for each of the six faces of the cube shaped volume. The form of Eq. (13) is well obeyed, but with a different value for the coefficient C. A fit to this data (see Fig. 14) yields

$$N_{3D} \approx 1.1502 \langle N_{2D} \rangle^{3/2} \tag{14}$$

Equation (14) provides the relationship necessary to convert between the size of 2D RVEs and SVEs in terms of number of grains and their 3D counterparts.

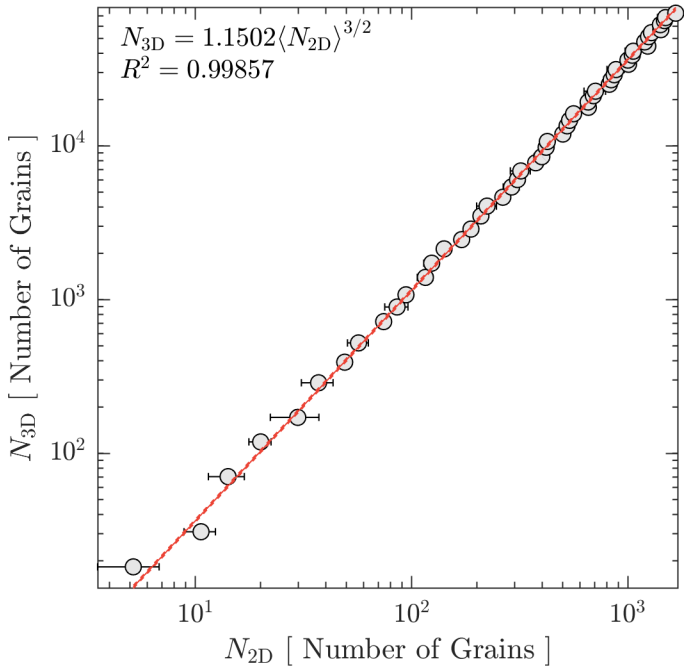

Figure 14: Comparison of the number of grains of realistic shape (i.e. non-convex) in a cube shaped volume (N_{3D}) and the number of grains appearing on its 2D faces (N_{2D}). The markers are the average, $\langle N_{2D}\rangle$, of all 6 cube faces, and the error-bars represent one standard deviation. The solid red line is the fit of Eq. (12) to obtain the value of $C = 1.1502$ for realistic (non-convex) grains. The dashed red lines (which fall nearly on top of the solid red line, indicating the excellent quality of the fit) are the 95% confidence intervals for the fit.

The strength of the stereological approach is that it makes "no assumptions about the geometry of the features being characterized" [45]. However, this requires that the elements of the SVE set are collected in such a way that they are statistically representative of the three-dimensional material. If a material consists of equiaxed grains then samples taken from a single plane are sufficient to characterize the structure and the sizes/cardinalities of RVEs and SVEs found in the present work apply directly.

Because we have expressed the RVEs and SVEs in terms of number of grains rather than units that have an explicit spatial scale (e.g. mm^2), the sizes of RVEs and SVEs found in the present work also hold for more general microstructures. In particular, the present results are also valid for 3D microstructures with anisometric (non-equiaxed) grains—in such cases the shape of the RVE becomes a rectangular prism (see Fig. 15)—and for microstructures with or without crystallographic texture. Thus there are a wide range of 3D microstructures for which the present results apply.

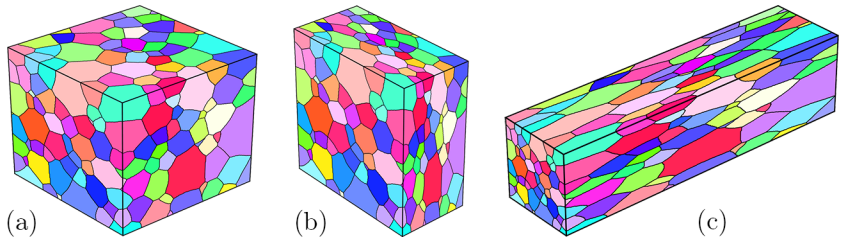

Figure 15: Examples of 3D microstructures for which the present results apply. These include, but are not limited to (a) isometric or equiaxed grains, (b) anisometric platelet shaped grains (shortened in one direction), and (c) anisometric needle shaped grains (elongated in one direction). Note that all three examples contain the same number of grains, and illustrate that if the grains are anisometric the RVE will be a rectangular prism.

Examples of three-dimensional microstructures for which the sizes of RVEs and SVEs found in the present work would not be guaranteed to apply are (i) heavily deformed microstructures in which grain shapes deviate strongly from those considered here, and (ii) those possessing *topological anisotropy*[3]—e.g. a microstructure in which the TJ fractions are different in different directions no matter what metric scaling (Fig. 15) is applied, and which would therefore require 2D SVE elements taken from multiple orientations.

4. Summary & Conclusions

The size of representative volume elements (RVEs) and the cardinality of statistical volume element (SVE) sets for 2D grain boundary networks (GBNs) were determined using both idealized honeycomb polycrystal models and more realistic polycrystal models resulting from front-tracking grain growth simulations.

It was observed that the RVE size varies across the space of triple junction (TJ) fractions, increasing as the TJ fraction approaches the J_0–J_3 edge. The size of RVEs for crystallographic texture were also determined for the same set of polycrystals and were found in most cases to be substantially smaller. However, the variations in RVE size across the space of TJ fractions were fundamentally different for texture and GBNs, and consequently relatively rare cases exist for which a GBN RVE may be smaller than the corresponding texture RVE, contrary to the general trend. Overall, depending on the permissible margin of error, GBNs required RVEs that were larger than for texture in 63%–82% of our observations, that were at least 50% larger than for texture in about half of our observations, and more than 3 times larger in 11%–20% of our observations. This suggests that the trend of GBNs requiring larger RVEs than for texture is significant in both frequency and magnitude.

The trend in the cardinality of SVE sets across the space of TJ fractions was qualitatively similar to that of the RVE sizes for both GBNs and texture.

We find that RVE sizes based on the idealized honeycomb templates significantly under-predict the texture RVE sizes for more realistic microstructures. However, the honeycomb idealization had on average roughly the same GBN RVE size as the more realistic grain growth templates. The reason that the GBN appears to be less negatively impacted by the honeycomb idealization was attributed to the smaller relative dispersion of the number of triple junctions per grain compared to the dispersion in the grain size distribution (i.e. the honeycomb template is topologically similar to realistic GBNs, but geometrically quite distinct).

We also observe that the size of an RVE and the cardinality of an SVE set both scale as a power law with the desired accuracy (the permissible margin of error). This suggests that the cost of increased accuracy is significant, highlighting the need to quantify necessary RVE sizes and SVE set cardinalities. In this context, the results of this work can help researchers to make an optimal trade-off between computational expense/experimental effort and quantitative accuracy.

The SVE cardinality was also found to scale as a power law with SVE sample size.

The figures and tables contained in this work facilitate the selection of an appropriate RVE size or cardinality of an SVE set for a given sample size, given a desired level of accuracy (margin of error between 1%–10%) and precision (what proportion of the distribution of RVE sizes/SVE set cardinalities over the J-space will be adequately represented).

To the best of the authors knowledge, this is the first time that RVEs and SVEs for GBNs have been systematically characterized. The results highlight the fact that, in a single microstructure, one charac-

[3]The stereological approach is valid even in the presence of anisotropy, but in such chases a valid SVE set would need to be constructed from samples taken from multiple orientations.

teristic or feature can be homogeneous (e.g. crystallographic texture) at a particular length scale while another is simultaneously heterogeneous (e.g. GBNs). The fact that GBN RVEs are substantially larger than those for crystallographic texture, in the same microstructures, suggests that the characteristic length-scale of heterogeneity in GBNs is most often naturally larger than for texture and special attention should be given to the choice of sample size when studying GBNs to ensure that results obtained from simulations and conclusions based upon experimental characterization are truly representative.

For texture, comparison to prior literature shows that the RVE sizes calculated in the present work are consistent with independently published values, and experimental measurements. As the present work represents the first characterization of GBN RVEs and SVEs, data for such a comparison are not yet available for GBNs.

Using stereological identities, we derived formulas (Eqs. (7), (9) and (14)) allowing for the prediction of 3D RVE and SVE sizes from the 2D values calculated in the present work. We showed that the present results can be adapted to 3D microstructures for a wide range of scenarios.

Here we summarize practical recommendations resulting from this work:

- The use of idealized honeycomb templates should generally be avoided, although this is more important when crystallographic texture is of greatest concern than when GBNs are of primary interest.
- Given the option, the use of an SVE set will always be more efficient than the use of an RVE for both GBNs and texture. It appears that there is always an SVE sample size for which this is true.
- As a rule of thumb, if a margin of error of 10% is permissible, 12 samples is a good initial guess for the cardinality of an SVE set for which each sample contains 10 grains (or 3 samples of 50 grains each).
- For experimental work, resource constraints may in some cases justify the use of an RVE instead of an SVE set (even though it is not the globally optimal solution in terms of efficiency). In this case, the results presented here aid in the selection of an appropriate RVE size.
- As a rule of thumb, if a margin of error of 10% is permissible, a sample containing roughly 200 grains should be a good initial guess for the required size of an RVE for both GBNs and texture.
- When characterizing TJ fractions in 2D microstructures, it is recommended that they be defined according to Eq. (3) to facilitate comparison with 3D microstructures.

5. Acknowledgements

We gratefully acknowledge the use of the supercomputing resources of the Office of Research Computing at Brigham Young University. Funding for this work was provided by the Department of Mechanical Engineering at Brigham Young University.

References

[1] D. T. Fullwood, S. R. Niezgoda, B. L. Adams, S. R. Kalidindi, Microstructure sensitive design for performance optimization, Progress in Materials Science 55 (6) (2010) 477–562. doi:10.1016/j.pmatsci.2009.08.002.
URL https://www.sciencedirect.com/science/article/pii/S0079642509000760?via%3Dihub

[2] S. Bargmann, B. Klusemann, J. Markmann, J. Eike, K. Schneider, C. Soyarslan, J. Wilmers, Progress in Materials Science Generation of 3D representative volume elements for heterogeneous materials : A review, Progress in Materials Science 96 (2018) 322–384. doi:10.1016/j.pmatsci.2018.02.003.
URL https://www.sciencedirect.com/science/article/pii/S0079642518300161?via%3Dihub

[3] T. Kanit, S. Forest, I. Galliet, V. Mounoury, D. Jeulin, Determination of the size of the representative volume element for random composites: Statistical and numerical approach, International Journal of Solids and Structures 40 (13-14) (2003) 3647–3679. doi:10.1016/S0020-7683(03)00143-4.
URL https://www.sciencedirect.com/science/article/pii/S0020768303001434?via%3Dihub

[4] I. Gitman, H. Askes, L. Sluys, Representative volume: Existence and size determination, Engineering Fracture Mechanics 74 (16) (2007) 2518–2534. doi:10.1016/j.engfracmech.2006.12.021.
URL http://www.sciencedirect.com/science/article/pii/S0013794406004772

[5] R. Hill, Elastic Properties of Reinforced Solids: Some Theoretical Principles (1963). doi:10.1016/0022-5096(63)90036-X.
URL https://www.sciencedirect.com/science/article/pii/002250966390036X

[6] P. Evesque, Fluctuations, Correlation and Representative Elementary Volume (REV) in Granular Materials, Poudres & Grains 11 (2005) 6–17.
URL https://arxiv.org/abs/cond-mat/0506385

[7] S. Mirkhalaf, F. M. Andrade Pires, R. Simoes, Determination of the size of the Representative Volume Element (RVE) for the simulation of heterogeneous polymers at finite strains, Finite Elements in Analysis and Design 119. doi:10.1016/j.finel.2016.05.004.
URL https://www.sciencedirect.com/science/article/pii/S0168874X16300750

[8] W. Drugan, J. Willis, A micromechanics-based nonlocal constitutive equation and estimates of representative volume element size for elastic composites, Journal of the Mechanics and Physics of Solids 44 (4) (1996) 497–524. doi:10.1016/0022-5096(96)00007-5.
URL https://www.sciencedirect.com/science/article/pii/0022509696000075

[9] S. K. Sebsadji, K. Chouicha, Determining periodic representative volumes of concrete mixtures based on the fractal analysis, International Journal of Solids and Structures 49. doi:10.1016/j.ijsolstr.2012.05.017.
URL https://www.sciencedirect.com/science/article/pii/S0020768312002193

[10] C. Huet, Application of variational concepts to size effects in elastic heterogeneous bodies, Journal of the Mechanics and Physics of Solids 38 (6) (1990) 813–841. doi:10.1016/0022-5096(90)90041-2.
URL https://www.sciencedirect.com/science/article/pii/0022509690900412

[11] A. El Moumen, T. Kanit, A. Imad, H. El Minor, Effect of reinforcement shape on physical properties and representative volume element of particles-reinforced composites: Statistical and numerical approaches, Mechanics of Materials 83 (2015) 1–16. doi:10.1016/j.mechmat.2014.12.008.
URL https://www.sciencedirect.com/science/article/pii/S016766361400221X?via%3Dihub

[12] W. M. Harris, W. K. Chiu, Determining the representative volume element size for three-dimensional microstructural material characterization. Part 1: Predictive models, Journal of Power Sources 282 (2015) 552–561. doi:10.1016/j.jpowsour.2015.02.035.
URL http://www.sciencedirect.com/science/article/pii/S037877531500258X

[13] H. Moussaddy, D. Therriault, M. Lévesque, Assessment of existing and introduction of a new and robust efficient definition of the representative volume element, International Journal of Solids and Structures 50 (24) (2013) 3817–3828. doi:10.1016/j.ijsolstr.2013.07.016.
URL https://www.sciencedirect.com/science/article/pii/S0020768313002965?via%3Dihub

[14] C. Schwarze, R. D. Kamachali, M. Kühbach, C. Mießen, M. Tegeler, L. Barrales-Mora, I. Steinbach, G. Gottstein, Computationally Efficient Phase-field Simulation Studies Using RVE Sampling and Statistical Analysis, Computational Materials Science 147 (2018) 204–216. doi:10.1016/j.commatsci.2018.02.005.
URL https://www.sciencedirect.com/science/article/pii/S0927025618300880?via%3Dihub

[15] M. Bouchedjra, C. Boulemia, A. Amrouche, Determination of the RVE size for polycrystal metals to predict monotonic and cyclic elastoplastic behavior : Statistical and numerical approach with new criteria, European Journal of Mechanics / A Solids 72 (2018) 1–15. doi:10.1016/j.euromechsol.2018.04.011.
URL https://www.sciencedirect.com/science/article/pii/S0997753817307799

[16] X. Yin, W. Chen, A. To, C. McVeigh, W. K. Liu, Statistical volume element method for predicting microstructure-constitutive property relations, Computer Methods in Applied Mechanics and Engineering 197 (43-44) (2008) 3516–3529. doi:10.1016/j.cma.2008.01.008.
URL https://www.sciencedirect.com/science/article/pii/S0045782508000339

[17] S. M. Qidwai, D. M. Turner, S. R. Niezgoda, A. C. Lewis, A. B. Geltmacher, D. J. Rowenhorst, S. R. Kalidindi, Estimating the response of polycrystalline materials using sets of weighted statistical volume elements, Acta Materialia 60 (13-14) (2012) 5284–5299. doi:10.1016/j.actamat.2012.06.026.
URL https://www.sciencedirect.com/science/article/abs/pii/S1359645412003989?via%3Dihub

[18] J. Zhang, K. Liu, C. Luo, a. Chattopadhyay, Crack initiation and fatigue life prediction on aluminum lug joints using statistical volume element-based multiscale modeling, Journal of Intelligent Material Systems and Structures 24 (17) (2013) 2097–2109. doi:10.1177/1045389X12457835.
URL http://jim.sagepub.com/cgi/doi/10.1177/1045389X12457835

[19] J. Zhang, K. Liu, A. Chattopadhyay, A Statistical Volume Element Based Approach to Multiscale Modeling of Fatigue Crack Formation in AA 2024-T351, in: 53rd AIAA/ASME/ASCE/AHS/ASC Structures, Structural Dynamics and Materials Conference 20th AIAA/ASME/AHS Adaptive Structures Conference 14th AIAA, 2012, pp. 1–10. doi:10.2514/6.2012-1538.
URL http://arc.aiaa.org/doi/abs/10.2514/6.2012-1538

[20] O. K. Johnson, L. Li, M. J. Demkowicz, C. A. Schuh, Inferring grain boundary structureproperty relations from effective property measurements, Journal of Materials Science 50 (21) (2015) 6907–

6919. doi:10.1007/s10853-015-9241-4.
URL http://link.springer.com/10.1007/s10853-015-9241-4

[21] B. W. Reed, M. Kumar, R. W. Minich, R. E. Rudd, Fracture roughness scaling and its correlation with grain boundary network structure, Acta Materialia 56 (13) (2008) 3278–3289. doi:10.1016/j.actamat.2008.03.019.
URL https://www.sciencedirect.com/science/article/abs/pii/S135964540800205X

[22] S. Bechtle, M. Kumar, B. P. Somerday, M. E. Launey, R. O. Ritchie, Grain-boundary engineering markedly reduces susceptibility to intergranular hydrogen embrittlement in metallic materials, Acta Materialia 57 (14) (2009) 4148–4157. doi:10.1016/j.actamat.2009.05.012.
URL https://www.sciencedirect.com/science/article/abs/pii/S1359645409003103?via%3Dihub

[23] L. Tan, K. Sridharan, T. R. Allen, R. K. Nanstad, D. A. McClintock, Microstructure tailoring for property improvements by grain boundary engineering, Journal of Nuclear Materials 374 (1-2) (2008) 270–280. doi:10.1016/j.jnucmat.2007.08.015.
URL https://www.sciencedirect.com/science/article/pii/S0022311507009646

[24] E. M. Lehockey, G. Palumbo, P. Lin, Improving the weldability and service performance of nickel- and iron-based superalloys by grain boundary engineering, Metallurgical and Materials Transactions A 29 (12) (1998) 3069–3079. doi:10.1007/s11661-998-0214-y.
URL http://www.springerlink.com/index/10.1007/s11661-998-0214-y

[25] H. Ma, F. La Mattina, I. Shorubalko, R. Spolenak, M. Seita, Engineering the grain boundary network of thin films via ion-irradiation: Towards improved electromigration resistance, Acta Materialia 123 (2017) 272–284. doi:10.1016/j.actamat.2016.10.040.
URL https://www.sciencedirect.com/science/article/abs/pii/S1359645416308084?via%3Dihub

[26] B. Koohbor, S. Ravindran, A. Kidane, Experimental determination of Representative Volume Element (RVE) size in woven composites, Optics and Lasers in Engineering 90 (2017) 59–71. doi:10.1016/j.optlaseng.2016.10.001.
URL https://www.sciencedirect.com/science/article/abs/pii/S0143816616302615?via%3Dihub

[27] A. Brahme, Y. Staraselski, K. Inal, R. K. Mishra, Determination of the Minimum Scan Size to Obtain Representative Textures by Electron Backscatter Diffraction, Metallurgical and Materials Transactions A 43 (13) (2012) 5298–5307. doi:10.1007/s11661-012-1364-5.
URL https://link.springer.com/article/10.1007/s11661-012-1364-5

[28] A. P. Tafti, A. B. Kirkpatrick, J. D. Holz, H. A. Owen, Z. Yu, 3DSEM: A 3D microscopy dataset, Data in Brief 6 (2016) 112–116. doi:10.1016/j.dib.2015.11.018.
URL https://www.sciencedirect.com/science/article/pii/S2352340915003133?via%3Dihub

[29] C. A. Schuh, M. Kumar, W. E. King, Analysis of grain boundary networks and their evolution during grain boundary engineering, Acta Materialia 51 (3) (2003) 687–700. doi:10.1016/S1359-6454(02)00447-0.
URL http://www.sciencedirect.com/science/article/pii/S1359645402004470

[30] M. E. Frary, C. A. Schuh, Correlation-space description of the percolation transition in composite microstructures, Physical Review E - Statistical, Nonlinear, and Soft Matter Physics 76 (4). doi:10.1103/PhysRevE.76.041108.
URL https://journals.aps.org/pre/abstract/10.1103/PhysRevE.76.041108

[31] M. Kumar, W. E. King, A. J. Schwartz, Modifications to the microstructural topology in f.c.c. materials through thermomechanical processing, Acta Materialia 48 (9) (2000) 2081–2091. doi:http://dx.doi.org/10.1016/S1359-6454(00)00045-8.
URL http://www.sciencedirect.com/science/article/pii/S1359645400000458

[32] V. Gertsman, M. Janecek, K. Tangri, Grain Boundary Ensembles in Polycrystals, Acta M 44 (7) (1996) 2869–2882. doi:10.1016/1359-6454(95)00396-7.
URL https://www.sciencedirect.com/science/article/abs/pii/1359645495003967

[33] C. Schuh, M. Frary, Correlations beyond the nearest-neighbor level in grain boundary networks, Scripta Materialia 54 (6) (2006) 1023–1028. doi:10.1016/j.scriptamat.2005.11.044.
URL https://www.sciencedirect.com/science/article/pii/S1359646205007955

[34] O. K. Johnson, C. A. Schuh, Texture mediated grain boundary network design in two dimensions, Journal of Materials Research 31 (9) (2016) 1171–1184. doi:10.1557/jmr.2016.138.
URL http://www.journals.cambridge.org/abstract_S0884291416001382

[35] E. A. Lazar, R. D. MacPherson, D. J. Srolovitz, A more accurate two-dimensional grain growth algorithm, Acta Materialia 58 (2) (2010) 364–372. doi:10.1016/j.actamat.2009.09.008.
URL http://www.sciencedirect.com/science/article/pii/S135964540900603X

[36] J. Levy, The Structure of High-Angle Grain Boundaries in Aluminium, physica status solidi (b) 31 (1) (1969) 193–201. doi:10.1002/pssb.19690310123.
URL https://onlinelibrary.wiley.com/doi/abs/10.1002/pssb.19690310123

[37] A. H. King, S. Shekhar, What does it mean to be special? The significance and application of the Brandon criterion, Journal of Materials Science 41 (23) (2006) 7675–7682. doi:10.1007/s10853-006-0665-8.
URL https://link.springer.com/article/10.1007/s10853-006-0665-8

[38] P. Davies, V. Randle, G. Watkins, H. Davies, Triple junction distribution profiles as assessed by electron backscatter diffraction, Journal of Materials Science 37 (19) (2002) 4203–4209. doi:10.1023/A:1020052306493.
URL https://link.springer.com/article/10.1023/A:1020052306493

[39] O. K. Johnson, J. M. Lund, T. R. Critchfield, Spectral graph theory for characterization and homogenization of grain boundary networks, Acta Materialia 146 (2018) 42–54. doi:10.1016/j.actamat.2017.11.054.
URL https://www.sciencedirect.com/science/article/abs/pii/S1359645417310455

[40] W. M. Harris, W. K. Chiu, Determining the representative volume element size for three-dimensional microstructural material characterization. Part 2: Application to experimental data, Journal of Power Sources 282 (2015) 622–629. doi:10.1016/j.jpowsour.2015.02.052.
URL http://www.sciencedirect.com/science/article/pii/S037877531500275X

[41] I. J. Hall, R. R. Praiiue, Non-Parametric Prediction Intervals, Journal of Quality Technology 7 (3) (1975) 109–114. doi:10.1080/00224065.1975.11980680.
URL https://www.tandfonline.com/doi/abs/10.1080/00224065.1975.11980680

[42] W. Q. Meeker, G. J. Hahn, L. A. Escobar, Statistical Intervals: A Guide for Practitioners and Researchers, 2nd Edition, John Wiley & Sons, Ltd, 2017.

[43] D. Freedman, P. Diaconis, On the histogram as a density estimator: L2 theory, Zeitschrift für Wahrscheinlichkeitstheorie und Verwandte Gebiete 57 (4) (1981) 453–476. doi:10.1007/BF01025868.
URL https://link.springer.com/article/10.1007%2FBF01025868?LI=true

[44] J. C. Russ, Practical Stereology, 1st Edition, Springer US, Boston, MA, 1986. doi:10.1007/978-1-4899-3533-5.
URL http://link.springer.com/10.1007/978-1-4899-3533-5

[45] J. C. Russ, R. T. Dehoff, Practical Stereology, 2nd Edition, Springer US, Boston, MA, 2000. doi:10.1007/978-1-4615-1233-2.
URL http://link.springer.com/10.1007/978-1-4615-1233-2

[46] J. Ohser, F. Mücklich, Statistical Analysis of Microstructures in Materials Science, John Wiley & Sons, Ltd, Chichester, West Sussex, 2000.

[47] E. E. Underwood, Quantitative stereology, Addison-Wesley Publishing Company, Reading, MA, 1970.

[48] O. K. Johnson, C. A. Schuh, The triple junction hull: Tools for grain boundary network design, Journal of the Mechanics and Physics of Solids 69 (2014) 2–13. doi:10.1016/j.jmps.2014.04.005.
URL https://www.sciencedirect.com/science/article/pii/S0022509614000659?via%3Dihub

[49] T. Baudin, R. Penelle, Determination of the total texture, Metallurgical Transactions A 24 (10) (1993) 2299–2311.

[50] E. Nakamachi, N. Tam, H. Morimoto, Multi-scale finite element analyses of sheet metals by using sem-ebsd measured crystallographic rve models, International Journal of Plasticity 23 (3) (2007) 450–489.

[51] F. E. Houdaigui, S. Forest, A. F. Gourgues, D. Jeulin, On the size of the representative volume element for isotropic elastic polycrystalline copper, in: IUTAM symposium on mechanical behavior and micro-mechanics of nanostructured materials, Springer, 2007, pp. 171–180.

[52] Y. Tadano, Polycrystalline behavior analysis of pure magnesium by the homogenization method, International Journal of Mechanical Sciences 52 (2) (2010) 257–265.

[53] K.-S. Zhang, Y.-K. Shi, J. W. Ju, Grain-level statistical plasticity analysis on strain cycle fatigue of a fcc metal, Mechanics of Materials 64 (2013) 76–90.

[54] S. I. Wright, M. M. Nowell, J. F. Bingert, A comparison of textures measured using x-ray and electron backscatter diffraction, Metallurgical and Materials Transactions A 38 (8) (2007) 1845–1855.

[55] M. Diehl, M. Groeber, C. Haase, D. A. Molodov, F. Roters, D. Raabe, Identifying structure–property relationships through dream. 3d representative volume elements and damask crystal plasticity simulations: An integrated computational materials engineering approach, JOM 69 (5) (2017) 848–855.

[56] T. Böhlke, R. Glüge, B. Klöden, W. Skrotzki, A. Bertram, Finite element simulation of texture evolution and swift effect in nial under torsion, Modelling and Simulation in Materials Science and Engineering 15 (6) (2007) 619.

[57] A. Prakash, S. Weygand, H. Riedel, Modeling the evolution of texture and grain shape in mg alloy az31 using the crystal plasticity finite element method, Computational Materials Science 45 (3) (2009) 744–750.

[58] L. Li, L. Shen, G. Proust, A texture-based representative volume element crystal plasticity model for predicting bauschinger effect during cyclic loading, Materials Science and Engineering: A 608 (2014) 174–183.

[59] M. A. Groeber, M. A. Jackson, DREAM.3D: A Digital Representation Environment for the Analysis of Microstructure in 3D, Integrating Materials and Manufacturing Innovation 3 (1) (2014) 56–72. doi:10.1186/2193-9772-3-5.
URL http://link.springer.com/10.1186/2193-9772-3-5